ADVANCED MATERIALS
www.advmat.de

Toward a Novel Energy-Dissipation Metamaterial with Tensegrity Architecture

Filipe A. Santos

The interest in novel energy-dissipation devices that offer advanced functionalities for optimal performance in state-of-the-art engineering applications is growing. In this regard, a highly tunable and innovative dissipator is developed. This dissipator features movement amplification capabilities resulting from the radial replication of a unit-cell with tensegrity architecture. The kinematic response of the dissipator is analyzed for several layouts, by varying the number of unit-cells within the device, their internal geometry, and identifying the corresponding locking configurations. A fully operational 3D-printed prototype is presented, demonstrating its excellent performance in terms of damping capabilities and feasibility. The experimental results are used to validate a numerical model of the flower unit. This model demonstrates the importance of pre-strain on the overall stiffness and dissipative features of the proposed system. By utilizing these numerical models, it is shown that the proposed device can be used as a building block for more complex assemblies such as periodic metamaterials with tensegrity architecture.

1. Introduction

Mechanical metamaterials are a new type of materials that have advanced functionalities and are often inspired by biological materials.[1] The designs of these materials have evolved from simple repeated unit-cells to increasingly complex geometries. The properties of mechanical metamaterials largely depend on the shape of the unit-cell and the interactions between them within the structure of the metamaterial.[2] These materials typically have a cellular structure that is optimized to enhance specific features such as wave propagation, stiffness, energy absorption, and shape morphing, while minimizing overall weight.[3–5] 3D-printing technologies, particularly those that use additive manufacturing, have recently allowed for the production of intricate geometries associated with these cellular structures.[6,7]

When the structural unit-cell of a metamaterial is a tensegrity, the resulting material is known as a tensegrity metamaterial.[8–13] A tensegrity structure is a system made up of cables and struts that rely on self-stress between tensioned and compressed members for stability.[14] Tensegrity structures that are pre-stressed are found at all scales in living systems and are well-suited for structures with deployable and variable geometries that can adapt to different condition.[15–17] The unique properties of tensegrity-based metamaterials, including lightweight design, high strength, customizability, resilience, and self-support, make them appealing for a variety of engineering applications.[18]

In this paper, we employ a planar Class-2 tensegrity unit-cell made up of four bars arranged in a rhombus shape and two perpendicular cables. This type of tensegrity is commonly referred to as D-bars,[19] which are lightweight and highly scalable systems that can effectively withstand compressive loads due to their optimized structural solutions in terms of mass. D-bars exhibit a pantographic effect owing to their geometry, which amplifies input displacements and enables their transversal ties to achieve higher strains. This feature is crucial when using D-bars as energy dissipation devices, as higher strains result in enhanced damping capabilities for the system.[20,21] As D-bars are closed structural systems, any pre-stress in the ties remains confined within the unit-cell and is not transmitted to the supports.

This paper introduces an innovative tensegrity-based energy dissipator that utilizes hysteretical re-centering forces in the ties. This device offers an exciting opportunity for new designs in the field of tensegrity metamaterials, as it can be customized with tailored pre-strains and incorporated into complex periodic assemblies. The device is obtained through radial replication of a D-bar unit-cell, resulting in a flower-shaped element with radial symmetry. The proposed device can solve the paradox of passive control systems by amplifying movement within the structure, making it effective even for small input displacements. A 3D-printed prototype has been developed, demonstrating the device's remarkable energy dissipation capabilities, lightness, and suitability for use in complex assemblies. This innovation has the potential to enable new low-cost, sustainable tensegrity metamaterial systems, with properties customized to specific engineering applications.

F. A. Santos
CERIS-NOVA, Department of Civil Engineering
NOVA School of Science and Technology, Universidade NOVA de Lisboa
Caparica 2829-516, Portugal
E-mail: fpas@fct.unl.pt

The ORCID identification number(s) for the author(s) of this article can be found under https://doi.org/10.1002/adma.202300639

DOI: 10.1002/adma.202300639

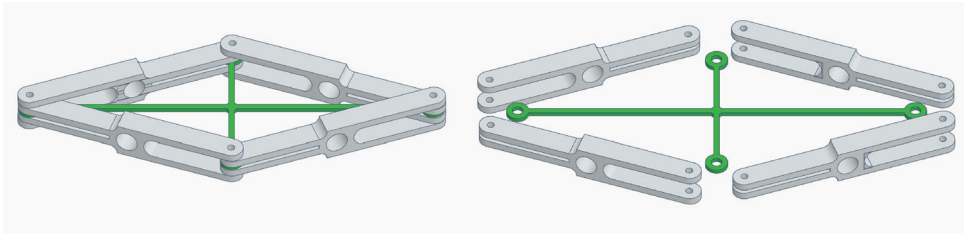

Figure 1. 3D views of a D-bar unit-cell.

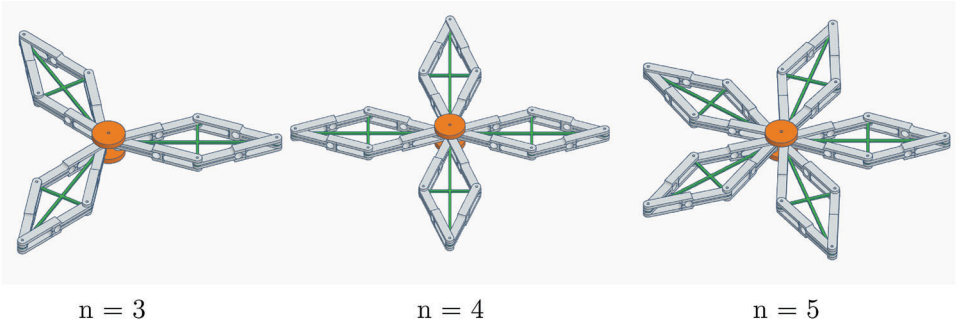

Figure 2. Examples of structures with radial symmetry obtained from the D-bar unit-cell.

2. Experimental Section

2.1. Flower Unit Design

D-bars may seem simple in theory, but their physical implementation poses some challenges, especially with regard to joint detailing. **Figure 1** presents a 3D view of the D-bar unit-cell and its constituent parts for assembly. The joint detailing allows for the relative rotation of the incoming struts and also restrains the corresponding end of the tie element. A single tie element with a cruciform shape was utilized to facilitate the interaction between the longitudinal and transverse ties, as the central points of these two segments remain fixed due to symmetry and do not exhibit relative displacement.

To create a flower-shaped structure with radial symmetry, one can replicate the D-bar unit-cell radially around one of its longitudinal ends. This results in a structure inscribed within a circle of radius R, which was equal to the length of the longitudinal tie. By varying the total number of D-bars within the flower, denoted as n, a range of different structures can be obtained. In this study, the focus was on three specific configurations, corresponding to $n = 3$, 4, and 5, which were shown in **Figure 2**.

To fully explore the potential of a tensegrity metamaterial, arrays of flower units can be created by replicating them along two dimensions, as shown in the process depicted in **Figure 3**.

To understand the behavior of a flower unit when its central node was displaced (u), it was necessary to analyze its kinematics and identify possible locking configurations that can occur when two adjacent struts overlap. This occurs when the angles between the struts (β and γ) become smaller than a certain threshold value (16° for the tested strut geometry, as shown in Figure 3b). The kinematics of a flower unit were characterized by the length of

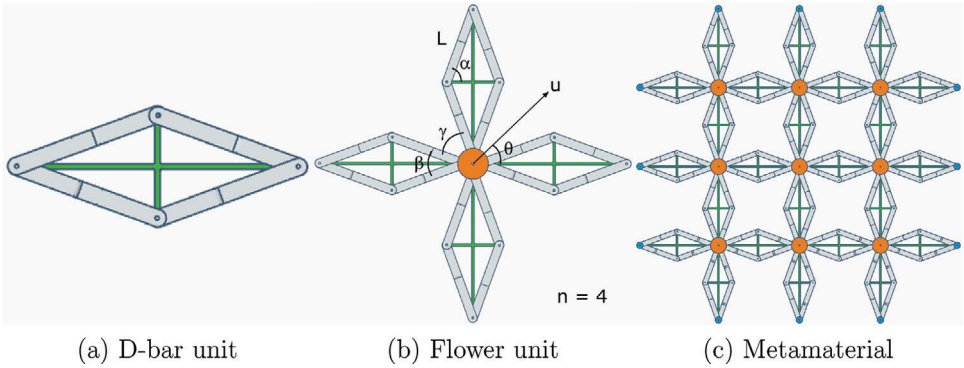

Figure 3. From a D-bar unit-cell to a tensegrity metamaterial.

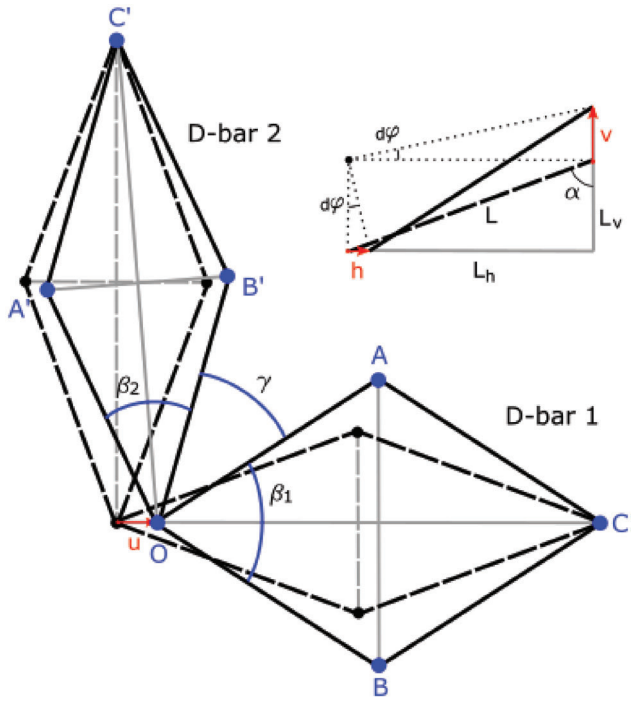

Figure 4. Kinematics of the flower unit.

the strut (L), the angle between the strut and the transversal tie of the D-bar unit-cell (α), the number of D-bars (n), and the angle θ formed between the displacement vector and the horizontal direction. **Figure 4** illustrates the interaction between two D-bars within a flower unit, assuming an arbitrary displacement u applied to the central node O with $\theta = 0$. Assume that the struts are axially indeformable and move as rigid bodies during the transformation of the flower unit, the kinematic compatibility can be expressed as follows:

$$L^2 = (L_h - h)^2 + (L_v + v)^2 = \text{const.} \quad (1)$$

In the small displacement regime, one obtains:

$$\frac{L_h}{L_v} = \frac{v}{h} = \tan(\alpha) \quad (2)$$

To determine the coordinates of the remaining points of the two D-bars shown in Figure 4, assume that points C and C' are fixed, and use Equation 2. After obtaining the full definition of the nodal coordinates of the D-bars, the lengths $\overline{A'B'}$, $\overline{B'A}$, and $\overline{AB}$ were computed. Finally, the law of cosines to determine the angles β_1, β_2, and γ was used.

A custom-written Matlab code was used to identify possible locking configurations using the described kinematic model. Due to symmetry, the kinematics of the flower units were studied by assuming $u > 0$ and letting θ vary in the interval $[0, 360/(2n)]$, where n is the number of D-bars within the unit. Locking configurations can be used to create smart materials with adaptive mechanical properties, which exhibit a large increase in stiffness and strength, with the onset of reversible locking transformations. These transformations are similar to jamming in granular materials, which exhibit tunable mechanical properties when the packing fraction of the particles increases. They can be used in a variety of applications, such as structured fabrics, impact absorption materials, and reconfigurable structures.[22–24] Compliant bistable structural elements also exhibit locking configurations and can be incorporated with a number of similar elements to create highly customizable multistable metamaterials with a large number of discrete stable configurations.[25,26] Three different D-bar configurations were selected for each flower unit (n = 3, 4, and 5), corresponding to α values of 60°, 65°, and 70° for the flower units with three and four D-bars. For the flower unit with five D-bars, α values of 62°, 66°, and 70° were chosen to ensure that the system does not lock at rest position. Some representative locking configurations for the tested flower assemblies are shown in **Figure 5**. Locking configurations are triggered within the D-bars when the β angle reaches its minimum threshold for the flower units with three and four D-bars, and by γ for the n = 5 flower unit.

To plot the displacement capacity of the tested flower units, the displacement value that triggers the locking configuration was normalized with respect to the strut length and shown as a function of the displacement angle θ in **Figure 6**. It should be noted that the displacement capacity of each flower unit was solely determined by its internal geometry.

2.2. Experimental Testing

To perform cyclic tests on a flower unit dissipator, a double-shear experimental testing apparatus was designed and built. Two physical models of flower units, each with four D-bars, were manufactured using a fused deposition modeling (FDM) 3D printer (Original Prusa i3 MK3S) and two different filaments.

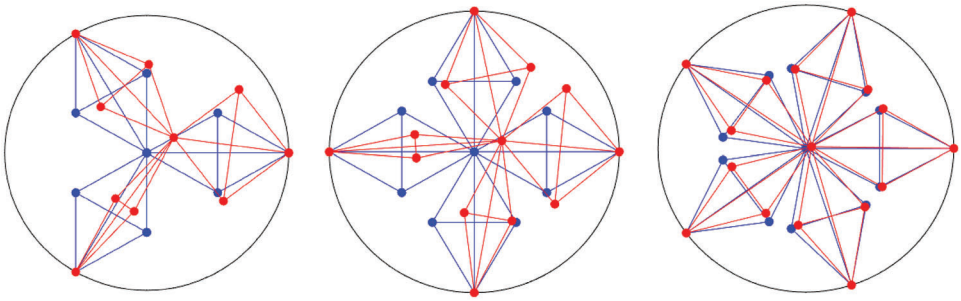

Figure 5. Selected locking configurations for the tested flower assemblies.

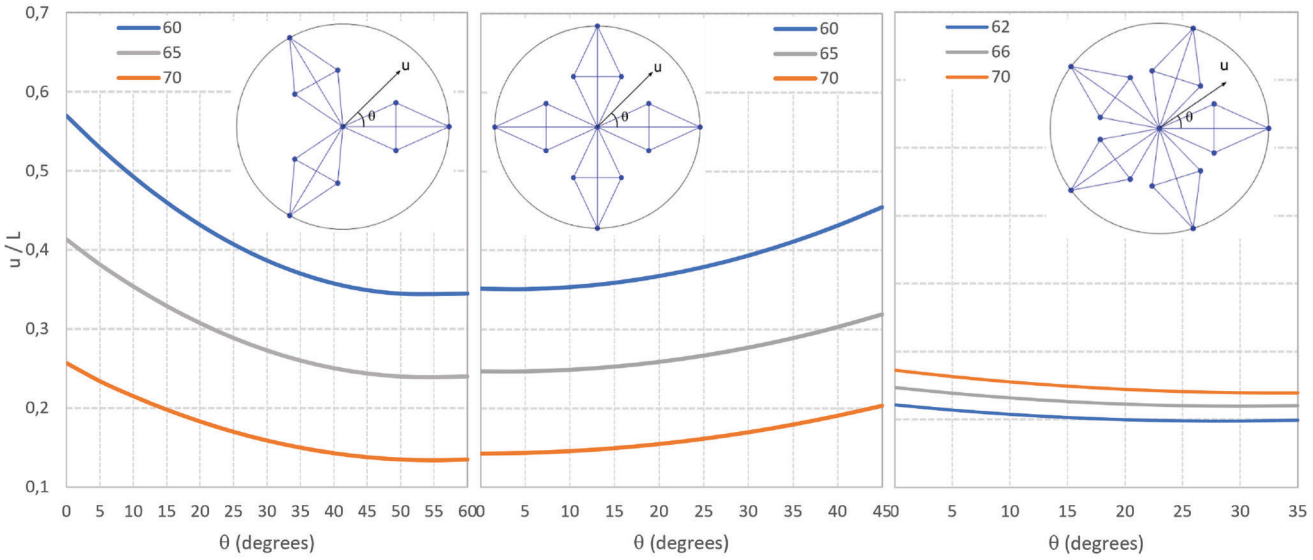

(a) 3 D-Bar Flower Unit (b) 4 D-Bar Flower Unit (c) 5 D-Bar Flower Unit

Figure 6. Normalized displacement capacity versus displacement angle.

Table 1. Material data.

Material	Density	Tensile modulus	Tensile strength
PETG	1.27 g cm^{-3}	1900 MPa	50 MPa
Filaflex 82A 'Original'	1.12 g cm^{-3}	22 MPa	45 MPa

Polyethylene terephthalate glycol (PETG) filament (Fillamentum) was used for the struts, while polyether–polyurethane elastomer (Filaflex 82A "Original") filament (Recreus) was used for the ties of the D-bars. The material properties of these filaments, retrieved from the technical datasheets provided by the suppliers, are compiled in **Table 1**.

Polyurethane-based filaments have already been successfully used by other authors in energy dissipation devices employing hysteretic damping.[27] The geometry of the flower unit is determined by the following parameters: $L = 140$ mm; $\alpha = 60°$; $n = 4$; $\theta = 45°$. The ties have a cross section of 4.0×3.0 mm^2 and exhibit no initial pre-strain. As per Figure 6b, the normalized displacement capacity for $\alpha = 60°$ and $\theta = 45°$ was 0.45. Multiplying this value by the strut length yields the prototype's displacement capacity, which was 63 mm, that is, the maximum displacement that does not activate locking configurations in the flower unit.

The experimental rig used for the testing was 3D printed in PETG, including all of the fixings and auxiliary parts. The actuator was provided by a Bosh Rexroth EMC 32-125 L100 OF01 precision rolled ball screw actuator, coupled with a SIGMA II Omron–Yaskawa cylindrical servomotor. The force transmitted to the prototype was monitored using a GEFRAN load-cell, model TU-K1C, connected to a National Instruments SCXI-1520 8-Channel Universal Strain Gage Input Module.

Figure 7 shows some photos of the experimental apparatus. To introduce the shear force, an auxiliary strut was placed between the two flower units, which transmitted the force to a steel dowel at the geometrical center of the modules. The dowel was equipped with a circular bearing support that could freely slide over the base plate and transmit any additional vertical force. The D-bars were pinned at the other extremities, and no additional weight was added to reduce friction.

The flower units underwent a series of triangular-shaped mechanical cycles, with maximum displacement amplitudes of 15, 30, and 45 mm and a loading frequency of up to 0.50 Hz, with marked stability, corresponding to speeds at the central node of the module of 30, 60, and 90 mm s^{-1}, respectively. **Figure 8** shows the flower units at rest and during mechanical cycling.

2.3. Mechanical Modeling

To characterize the nonlinear tensile stress-strain response of the Filaflex material, a test coupon was 3D printed and tested on a Zwick–Roell Z050 universal test machine. The test was conducted up to a total strain of 100% at a strain rate of 0.7 s^{-1} to apprehend the behavior of the Filaflex ties associated with fast dynamic loadings. **Figure 9**a shows the perfectly elastic-plastic constitutive model, which was adequately tuned to obtain the same amount of energy dissipating capabilities as in the experimental curve. The areas enclosed by the numerical and experimental hysteresis were matched to achieve this goal.

When subjected to compression, the ties become slack and cease to contribute to the overall stiffness of the system. By pre-straining the ties, it was possible to shift the origin of the force–displacement graphs, enabling the ties to cope with a certain degree of compression, which depends on the introduced pre-strain. Figure 9b shows the influence of the initial pre-strain on the force–displacement relationship exhibited by the transversal ties. As the pre-strain increases, the force–displacement graph moves toward the left-hand bottom corner of the plot.

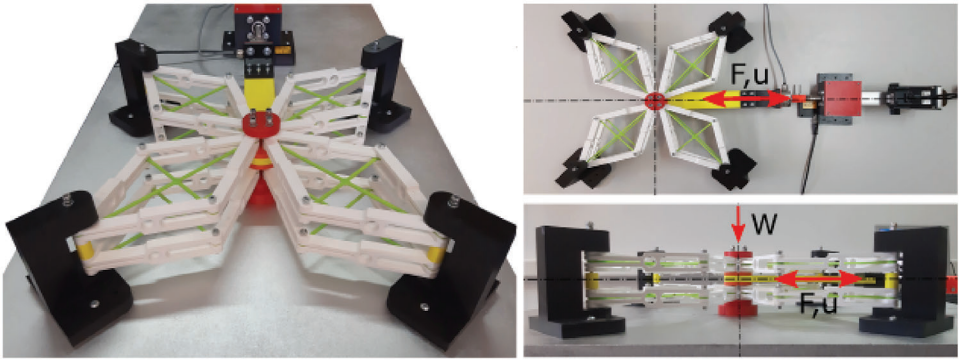

Figure 7. Experimental validation of a physical mode with a double-shear apparatus.

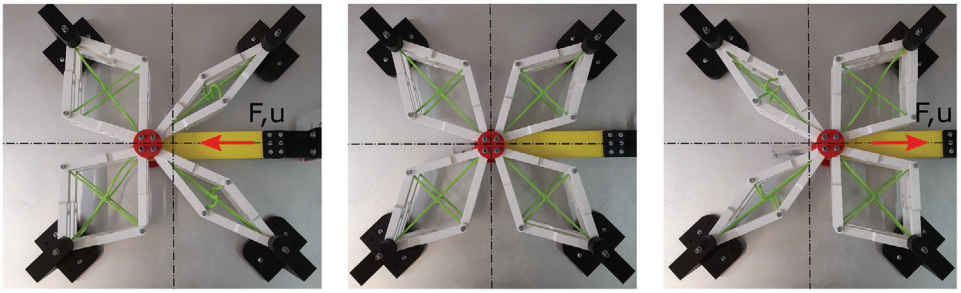

Figure 8. General kinematics of the tested prototype.

The cyclic response of the proposed flower unit dissipators was simulated using the Structural Analysis Program SAP2000 by running a direct-integration time-history analysis. The struts were modeled as axially undeformable frame elements, and the ties were modeled as multi-linear plastic link elements, as shown in Figure 9b. A triangular-shaped displacement input was used to control the load introduction at the central node of the flower units. The longitudinal nodes of the D-bars were fixed, while the transversal nodes were free to move and rotate.

It is worth noting that the proposed computational approach may become less tractable as the size of the tensegrity-based metamaterial increases. The tractability of a method depends on various factors, such as the model's complexity, available computational resources, and required accuracy level. The computational complexity of tensegrity-based metamaterials can increase rapidly with their size, which can make some methods less suitable. To address this limitation, highly efficient computational mechanical methods have been developed to simulate extremely large metamaterials with improved tractability.[28]

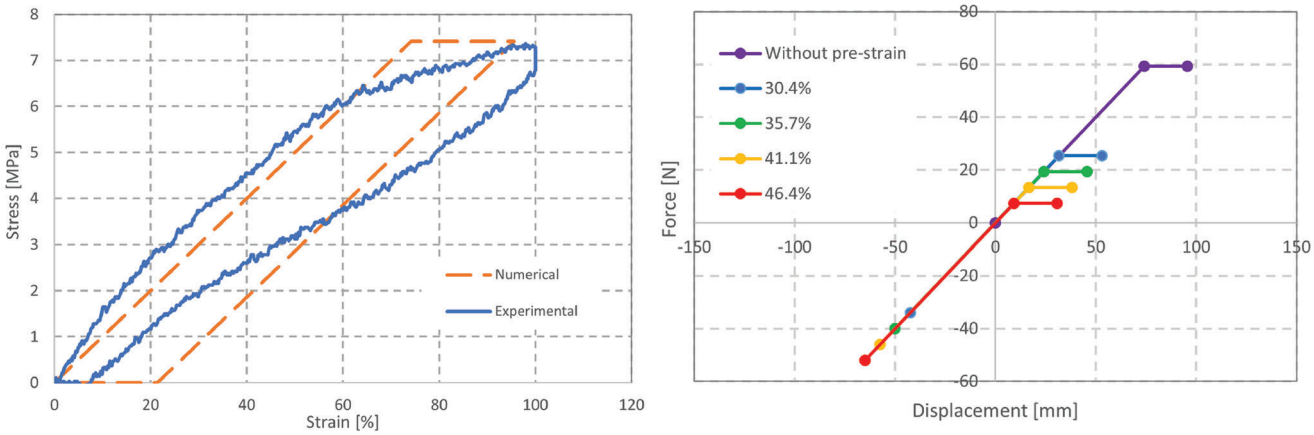

(a) Stress-strain responses

(b) Pre-strain effect

Figure 9. Constitutive relationships for the Filaflex ties.

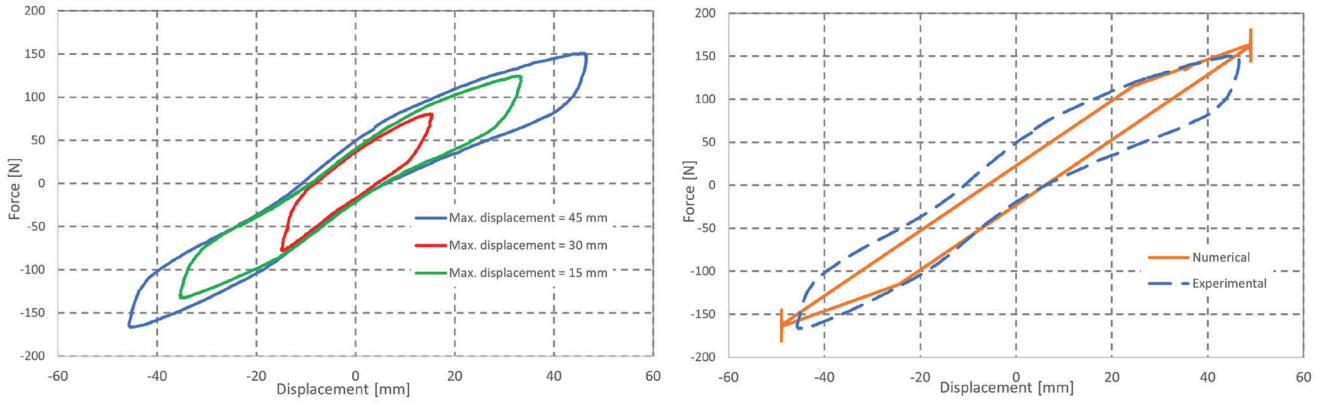

(a) Experimental responses

(b) Experimental vs. numerical responses

Figure 10. Force–displacement responses for a loading frequency of 0.50 Hz.

3. Results and Discussion

Figure 10 shows the experimental and numerical results for the shear force F versus lateral displacement u responses of the prototype, for all the tested amplitudes.

Figure 10b displays the force–displacement response obtained from the numerical model in comparison with the experimental curve. The two curves show good approximation, especially on the negative branch of the hysteresis. By calculating the equivalent viscous damping of both curves, using $\zeta_{eq} = E_D/(4\pi D)$, where E_D represents the dissipated energy and D is the elastic strain energy, we obtain 10% and 17% for the numerical and experimental hysteresis, respectively. This difference may arise from the numerical model's neglect of the dissipation due to friction between the interfaces of the prototype.

Using the validated numerical model, we conducted a series of parametric studies to test various configurations for the flower units. **Figure 11** presents a compilation of the cyclic force–displacement responses of the tested flower units, both with and without an initial pre-strain in the corresponding ties (ϵ_0 = 35.7%). The amplitude of the imposed cyclic displacement is adjusted to match the displacement capacity of each unit and, in the cases with an initial pre-strain, to ensure that the ties do not become slack.

In Figure 11a, it can be observed that the flower unit with three D-bars, without an initial pre-strain, exhibits poor behavior. The lack of symmetry along the vertical axis results in different responses for positive and negative displacements. This issue is somewhat resolved by introducing pre-strain in the ties. However, the hysteresis size remains limited, as shown in Figure 11b. The flower unit with four D-bars, due to its bi-symmetry, displays stable behavior for all directions. Pre-strain enables the system to increase the area of the force–displacement hysteresis and, hence, enhances its ability to dissipate energy (see Figure 11c,d). By computing ζ_{eq}, the flower units with and without pre-strain yield values of 15% and 10%, respectively.

The system with five D-bars lacks overall mobility, resulting in mostly linear behavior without the ability to dissipate energy (see Figure 11e,f). In all tested flower units, introducing pre-strain prevents the ties from slackening, leading to flower units with increased stiffness. Pre-strain, therefore, can be used as a powerful tool to control the stiffness of the proposed metamaterial with tensegrity-based architecture.

Since the flower unit with four D-bars exhibits the best overall behavior among all tested flower units, an additional study on the influence of displacement amplitude and initial pre-strain on its damping capabilities was conducted. The flower unit, with different levels of initial pre-strain (as shown in Figure 9b), was subjected to mechanical cycles of growing amplitude, with u_{max} ranging from 10 to 50 mm. The resulting force–displacement relationships are plotted in **Figure 12**, along with the corresponding computed equivalent viscous damping values.

When the displacement is small, the flower unit has limited energy dissipation capacity. As the displacement increases, the system's equivalent viscous damping also increases. However, pre-strain can improve the system's damping capabilities.

To compare, commercial elastomeric isolators typically have an equivalent viscous damping of 15% at 100% shear strain (HDRB) by alternating high damping rubber compound with steel laminates and joining them through vulcanization. The proposed tensegrity-based metamaterial has a maximum equivalent viscous damping of 23%, which is 53% higher than HDRB.[29]

To demonstrate the potential and versatility of the proposed flower assembly scheme as a tensegrity metamaterial, two simulations of a 3×3 array are presented. The array is built with four D-bars flower units. In the first simulation, the displacement is introduced at the central node of the assembly. In the second simulation, the displacement is introduced at eight different units adjacent to the central module. The exterior nodes of the array are restrained for both simulations.

Figure 13a,b shows the force–displacement diagrams of the metamaterial system for the first and second simulations, respectively. In both cases, the strain ϵ_0 is 35.7

The force–displacement diagrams obtained from the simulations clearly demonstrate that the proposed tensegrity metamaterial can offer a wide range of mechanical responses by appropriately selecting the input parameters. In the first example, the device exhibits increased flexibility, enabling it to accommodate larger displacements than the single flower unit with four D-bars while still retaining its energy dissipation capability. In the

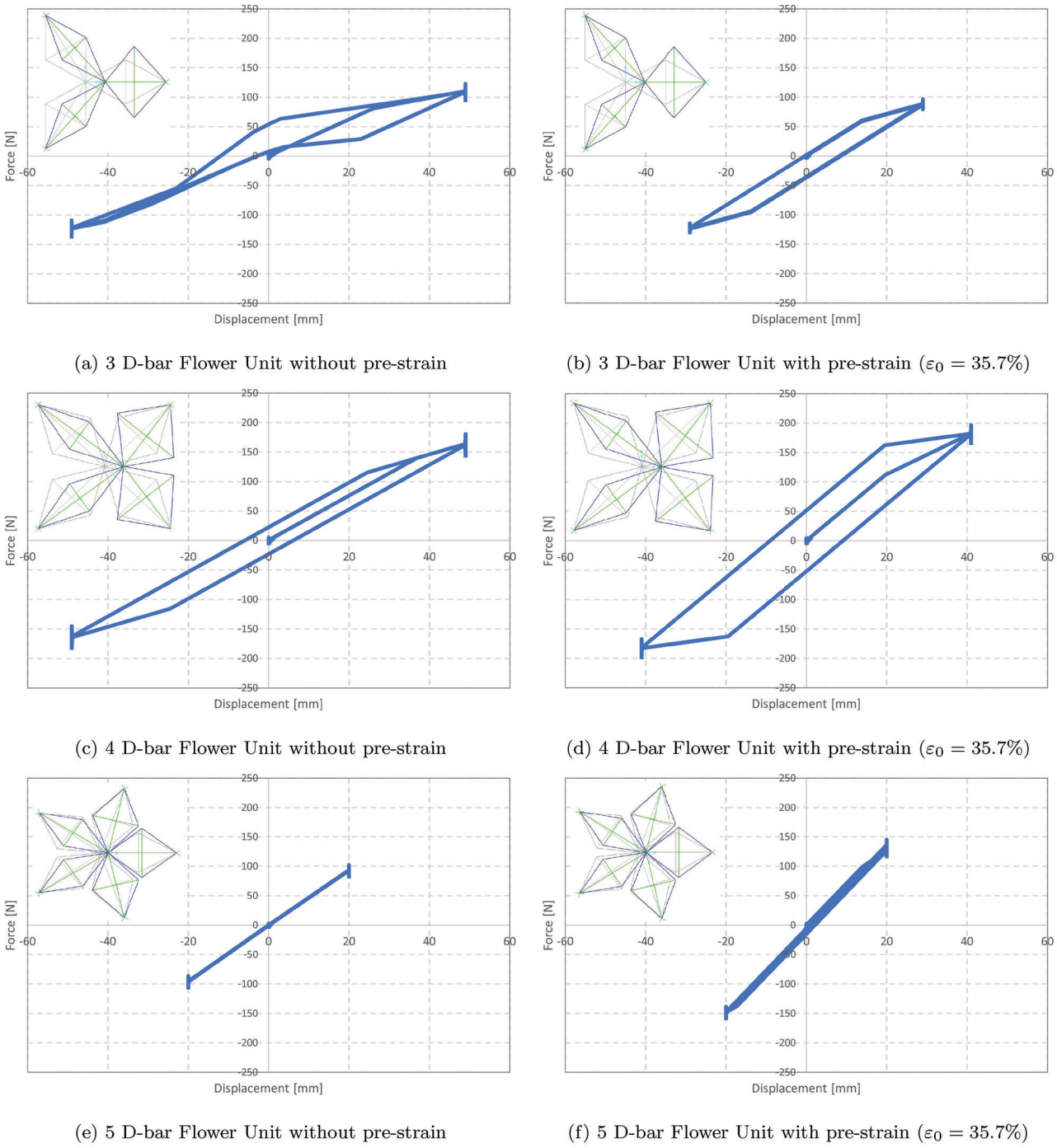

(a) 3 D-bar Flower Unit without pre-strain

(b) 3 D-bar Flower Unit with pre-strain ($\varepsilon_0 = 35.7\%$)

(c) 4 D-bar Flower Unit without pre-strain

(d) 4 D-bar Flower Unit with pre-strain ($\varepsilon_0 = 35.7\%$)

(e) 5 D-bar Flower Unit without pre-strain

(f) 5 D-bar Flower Unit with pre-strain ($\varepsilon_0 = 35.7\%$)

Figure 11. Cyclic force–displacement responses of the flower units.

second example, the device displays higher stiffness and can mobilize higher force thresholds, also with high damping capabilities ($\zeta_{eq} = 20\%$).

Due to its scalability, which allows it to be modified in size, the device's potential applications are vast, spanning from mechanical and aerospace to civil engineering structures. In terms of the latter, the device could be used as a seismic isolator. Seismic isolators have two key features, namely frequency tuning and damping, both of which the proposed device can easily address.

4. Conclusion

This work has provided additional insights into the development of novel energy dissipation devices with tensegrity architectures that can serve as building blocks for more complex assemblies,

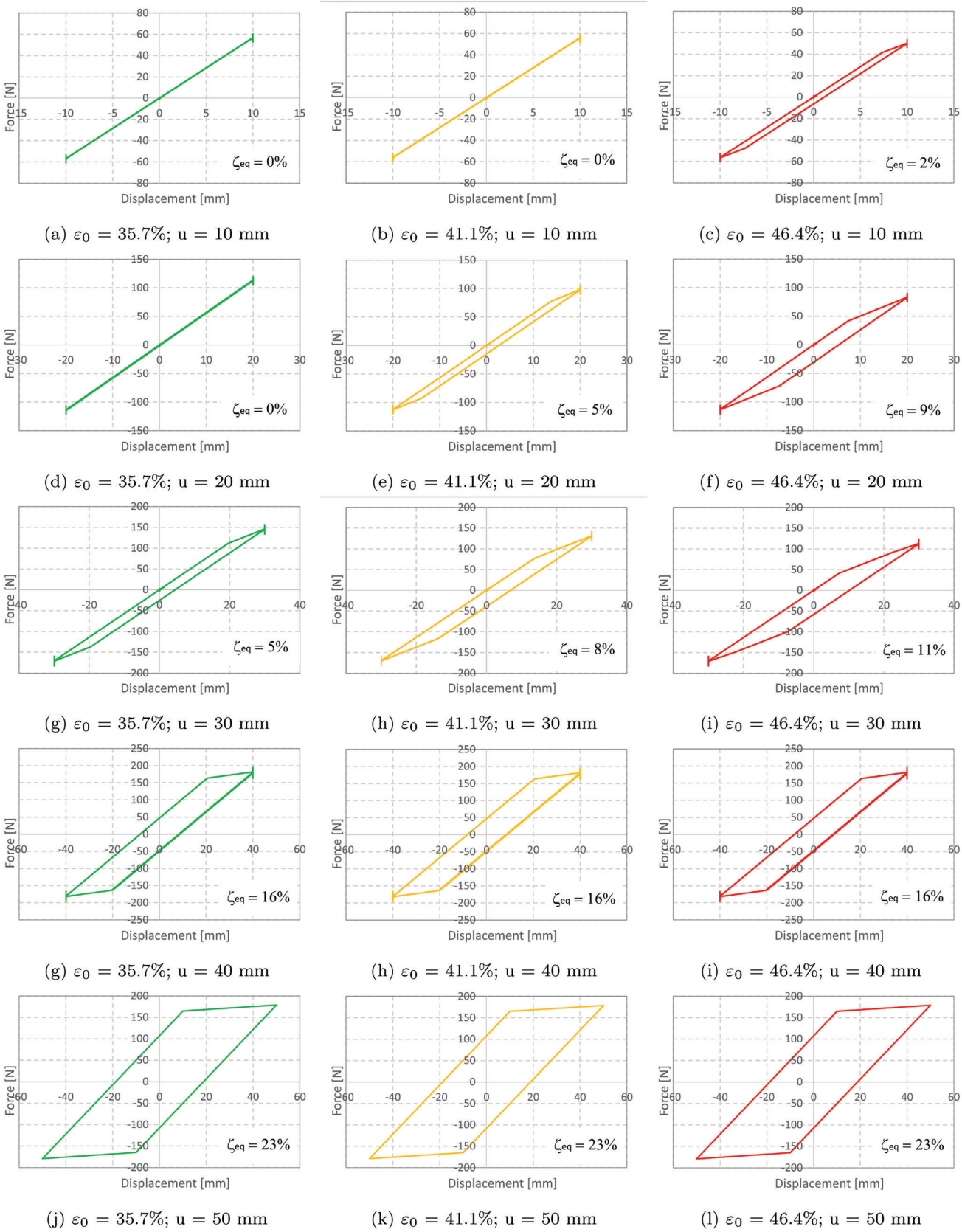

(a) $\varepsilon_0 = 35.7\%$; u = 10 mm (b) $\varepsilon_0 = 41.1\%$; u = 10 mm (c) $\varepsilon_0 = 46.4\%$; u = 10 mm

(d) $\varepsilon_0 = 35.7\%$; u = 20 mm (e) $\varepsilon_0 = 41.1\%$; u = 20 mm (f) $\varepsilon_0 = 46.4\%$; u = 20 mm

(g) $\varepsilon_0 = 35.7\%$; u = 30 mm (h) $\varepsilon_0 = 41.1\%$; u = 30 mm (i) $\varepsilon_0 = 46.4\%$; u = 30 mm

(g) $\varepsilon_0 = 35.7\%$; u = 40 mm (h) $\varepsilon_0 = 41.1\%$; u = 40 mm (i) $\varepsilon_0 = 46.4\%$; u = 40 mm

(j) $\varepsilon_0 = 35.7\%$; u = 50 mm (k) $\varepsilon_0 = 41.1\%$; u = 50 mm (l) $\varepsilon_0 = 46.4\%$; u = 50 mm

Figure 12. Force–displacement relationships. Influence of pre-strain and displacement amplitude on the damping capabilities of the flower unit with four D-bars.

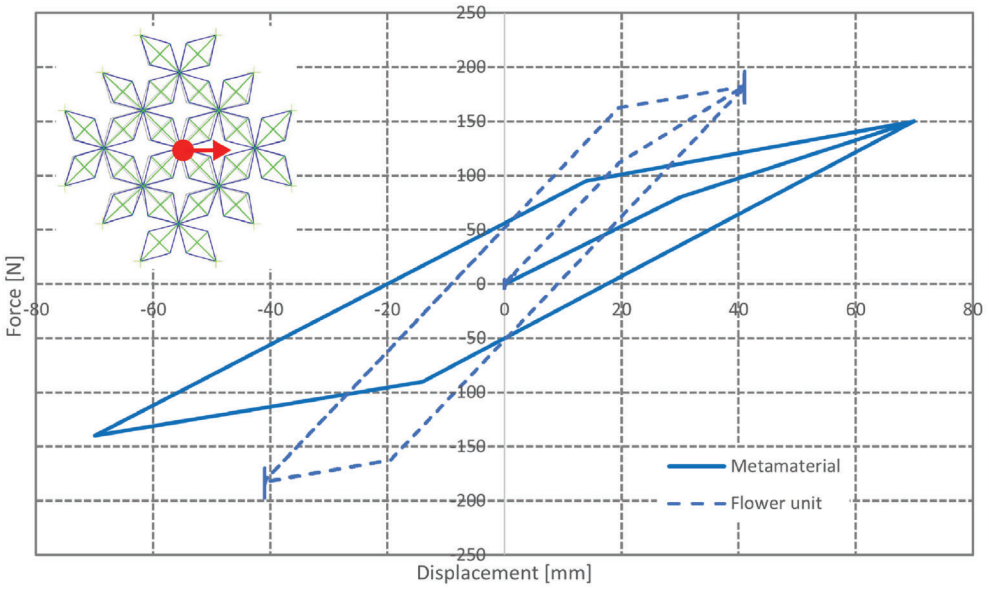

(a) Metamaterial with one central activation point.

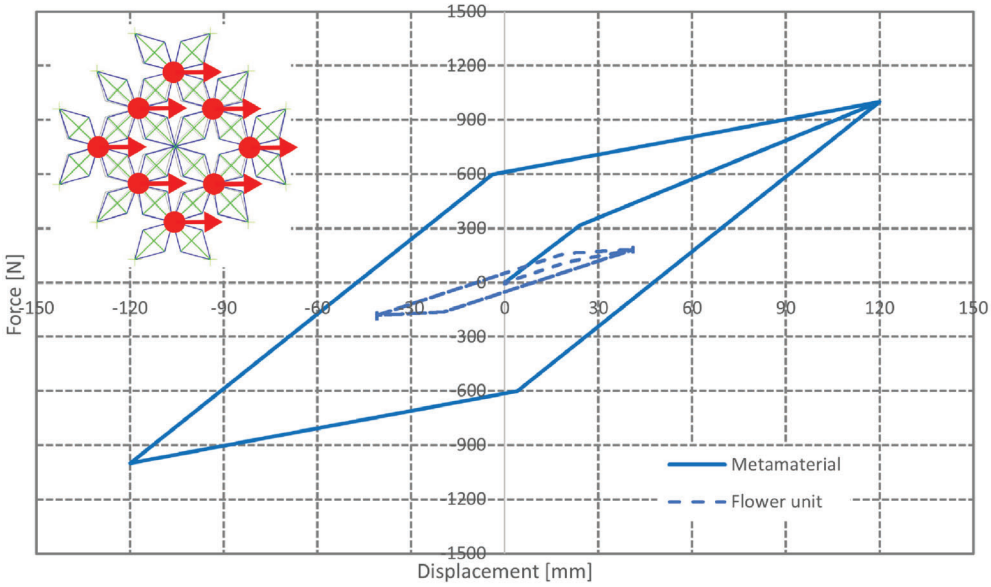

(b) Metamaterial with eight activation points.

Figure 13. Tensegrity metamaterial force–displacement diagrams.

such as periodic metamaterials. The proposed device is highly tunable and can be manufactured with custom-made properties using standard 3D printers. Its main advantage over current counterparts is its versatility and scalability as a standalone device.

Starting from the geometry of the D-bar unit cell, which can be optimized to yield a specific displacement amplitude or amplification, to the composition and initial pre-strain of the flower unit, which mainly determines its damping capabilities and stiffness, and finally considering the possibility of using a periodic assembly comprising an array of flower units, one has significant control over the device's overall performance. This enables tailoring its properties to meet specific design requirements.

Supporting Information

Supporting Information is available from the Wiley Online Library or from the author.

Acknowledgements

This work was part of the research activity carried out at Civil Engineering Research and Innovation for Sustainability (CERIS) and has been funded

by Fundação para a Ciância e a Tecnologia (FCT) in the framework of project UIDB/04625/2020.

Conflict of Interest

The author declares no conflict of interest.

Data Availability Statement

The data that support the findings of this study are available from the corresponding author upon reasonable request.

Keywords

3D printing, D-bars, energy dissipation, metamaterials, tensegrity

Received: January 19, 2023
Revised: March 16, 2023
Published online: May 5, 2023

[1] F. Barthelat, *Int. Mater. Rev.* **2015**, *60*, 413.
[2] J. Christensen, M. Kadic, M. Wegener, O. Kraft, *MRS Commun.* **2015**, *5*, 453.
[3] E. Barchiesi, M. Spagnuolo, L. Placidi, *Math. Mech. Solids* **2019**, *24*, 212.
[4] S. A. Cummer, J. Christensen, A. Alù, *Nat. Rev. Mater.* **2016**, *1*, 16001.
[5] M. Kadic, G. W. Milton, M. van Hecke, M. Wegener, *Nat. Rev. Phys.* **2019**, *1*, 198.
[6] A. Amendola, E. H. Nava, R. Goodall, I. Todd, R. E. Skelton, F. Fraternali, *Compos. Struct.* **2015**, *131*, 66.
[7] F. A. Santos, H. Rebelo, M. Coutinho, L. S. Sutherland, C. Cismasiu, I. Farina, F. Fraternali, *Compos. Struct.* **2021**, *256*, 113128.
[8] A. Amendola, A. Krushynska, C. Daraio, N. M. Pugno, F. Fraternali, *Int. J. Solids Struct.* **2018**, *155*, 47.
[9] J. J. Rimoli, R. K. Pal, *Composites, Part B* **2017**, *115*, 30.
[10] A. Micheletti, G. Ruscica, F. Fraternali, *Nonlinear Dyn.* **2019**, *98*, 2737.
[11] J. Bauer, J. A. Kraus, C. Crook, J. J. Rimoli, L. Valdevit, *Adv. Mater.* **2021**, *33*, 2005647.
[12] Y. Wang, W. Zhao, J. J. Rimoli, R. Zhu, G. Hu, *Extreme Mech. Lett.* **2020**, *37*, 100724.
[13] J. Zhang, M. Ohsaki, J. J. Rimoli, K. Kogiso, *Compos. Struct.* **2021**, *267*, 113903.
[14] R Motro, *Int. J. Space Struct.* **1992**, *7*, 75.
[15] T. Liedl, B. Högberg, J. Tytell, D. E. Ingber, W. M. Shih, *Nat. Nanotechnol.* **2010**, *5*, 520.
[16] S. Li, K.-Yen Hsieh, Chiao-I Kuo, S.-Hui Lee, G. D. Pintilie, K. Zhang, Chung-I Chang, *Sci. Adv.* **2021**, *7*, eabj7835.
[17] L.-Y. Zhang, Y. Zheng, X. Yin, S. Zhang, H.-Q. Li, G.-K. Xu, *Mech. Mach. Theory* **2022**, *173*.
[18] A. Micheletti, P. P. Guidugli, *Arch. Appl. Mech.* **2022**, *92*, 2525.
[19] R. E. Skelton, M. C. de Oliveira, *Tensegrity Systems*, Springer, Boston, MA, USA **2009**.
[20] F. Fraternali, F. Santos, *Extreme Mech. Lett.* **2019**, *33*, 100578.
[21] F. A. Santos, C. Carooç, A. Amendola, M. Miniaci, F. Fraternali, *Int. J. Multiscale Comput. Eng.* **2022**, *20*, 53.
[22] Y. Wang, L. Li, D. Hofmann, J. E. Andrade, C. Daraio, *Nature* **2021**, *596*, 238.
[23] Y. Wang, B. Ramirez, K. Carpenter, C. Naify, D. Hofmann, C. Daraio, *Extreme Mech. Lett.* **2019**, *33*, 100557.
[24] P. A.-Lindström, J. Willmann, S. Tibbits, F. Gramazio, M. Kohler, *Granular Matter* **2016**, *18*, 28.
[25] M. Santer, S. Pellegrino, *Int. J. Solids Struct.* **2008**, *45*, 6190.
[26] C. Intrigila, A. Micheletti, N. A. Nodargi, E. Artioli, P. Bisegna, *Addit. Manuf.* **2022**, *57*, 102946.
[27] F. Fraternali, N. Singh, A. Amendola, G. Benzoni, G. W. Milton, *Nonlinear Dyn.* **2021**, *106*, 3147.
[28] X. Yin, B.-Cong Wang, L. Liu, L.-Yuan Zhang, G.-K. Xu, *J. Mech. Phys. Solids* **2022**, *169*, 105077.
[29] J. M. Kelly, *Earthquake-Resistant Design with Rubber*, Springer, London, UK **1997**.